Related Articles

Line-source excitation of realistic conformal metasurface cloaks
J. Appl. Phys. 112, 104902 (2012)

High-performance solution-processed plasmonic Ni nanochain-Al2O3 selective solar thermal absorbers
Appl. Phys. Lett. 101, 203109 (2012)

Infrared characteristics of VO2 thin films for smart window and laser protection applications
Appl. Phys. Lett. 101, 191905 (2012)

Fredholm's equations for subwavelength focusing
J. Math. Phys. 53, 103520 (2012)

Dual-band asymmetry chiral metamaterial based on planar spiral structure
Appl. Phys. Lett. 101, 161901 (2012)

Additional information on Appl. Phys. Lett.

Journal Homepage: http://apl.aip.org/
Journal Information: http://apl.aip.org/about/about_the_journal
Top downloads: http://apl.aip.org/features/most_downloaded
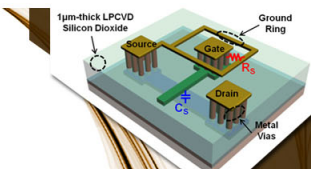Information for Authors: http://apl.aip.org/authors

Polarization-insensitive and wide-angle plasmonically induced transparency by planar metamaterials

Xiaoyang Duan,[1] Shuqi Chen,[1,a)] Haifang Yang,[2] Hua Cheng,[1] Junjie Li,[2] Wenwei Liu,[1] Changzhi Gu,[2] and Jianguo Tian[1,b)]

[1]*The Key Laboratory of Weak Light Nonlinear Photonics, Ministry of Education, School of Physics and Teda Applied Physics School, Nankai University, Tianjin 300071, China*
[2]*Beijing National Laboratory for Condensed Matter Physics, Institute of Physics, Chinese Academy of Sciences, P. O. Box 603, Beijing 100190, China*

We present the design, characterization, and experimental demonstration of a polarization-insensitive wide-angle plasmonically induced transparency (PIT) planar metamaterial (MM) in the near-infrared regime. A four-level plasmonic system is proposed to explain and analyze the forming mechanisms of the PIT planar MM, whose results agree closely with the simulated and experimental results. This shows that the local asymmetrical nanostructure leading to the plasmon-assisted interaction is the key to producing PIT, but it does not mean that PIT cannot be achieved by the whole symmetrical nanostructure. This work offers a further step in developing optical modulation. © *2012 American Institute of Physics.* [http://dx.doi.org/10.1063/1.4756944]

Plasmonically induced transparency (PIT) in metamaterials (MMs) is a fascinating phenomenon that mimics quantum interference of electromagnetically induced transparency (EIT) in laser-driven atomic systems.[1–6] This phenomenon opens a narrow transparency window within a transmission stop band through a highly efficient plasmon coupling between two artificially resonant elements, where bright mode energy is transformed into dark mode. It has been found that PIT underlies many particular useful applications, such as slow light,[7] sensing,[8,9] and optical switching.[10] Being different from other methods showing the classical analogue of EIT such as mechanical oscillators,[11] split-ring resonators,[12] optical resonators,[13,14] and metallic nanoparticle arrays,[15] PIT is an excellent example of merging between plasmonics and MMs. This lays the foundation for manipulating light by using metal nanostructures to achieve effective EIT-like optical properties for media. Because of the inherent limitations in applying EIT, PIT has received much attention due to the prominent advantages of room temperature manipulability, artificially controlling spectral response, and the ability to integrate with nanoplasmonic circuits.

In spite of many obvious advantages, the previously designed PIT devices principally have an inherent drawback. They strongly depend on the polarization and angle of incident waves on the asymmetry of the structures. Most studies show that introducing a broken symmetry to the spatial arrangement of the bright and dark resonators is a prerequisite for PIT,[1–5] since the asymmetry permits excitation of the otherwise forbidden dark mode. The degree of asymmetry determines the coupling strength of the bright and dark modes. Therefore, the previous devices also strongly depend on the incident angle.

In this letter, we present the design, characterization, and experimental demonstration of a PIT planar MM in the near-infrared regime. We demonstrate that PIT can be achieved by symmetrical planar MMs. Meanwhile, a four-level plasmonic system is proposed to explain and analyze the forming mechanisms of the PIT planar MM, whose results agree with the simulated and experimental results. The PIT planar MM is polarization-insensitive, and the transparency window remains high with large incident angles for both transverse electric (TE) and transverse magnetic (TM) configurations.

Motivated by the drawbacks mentioned above, here we propose a PIT planar MM fabricated on a quartz substrate, in which the top metallic layer consists of four rotationally aligned "=" pairs (see Fig. 1(a)). Based on the concept of EIT in atomic physics, we use a general description of an EIT-like plasmonic system (see Fig. 1(b)) to demonstrate and quantitatively describe the near-field coupling among meta-atoms.[1–3] Corresponding to the geometric position of the gold bars, the system consists of three artificial states, a radiative plasmonic state $|1\rangle = \tilde{A}_1(\omega)e^{i\omega t}$ (bright mode), a dark plasmonic state $|2\rangle = \tilde{A}_2(\omega)e^{i\omega t}$ (dark mode), and an additional plasmonic state $|3\rangle = \tilde{A}_3(\omega)e^{i\omega t}$ (additional mode), which have resonant frequencies ω_{01}, ω_{02}, ω_{03}, and damping factors γ_1, γ_2, γ_3, respectively. The damping factors combine radiative and non-radiative damping due to the intrinsic loss. A four-level plasmonic system is formed by three states of coupled meta-atoms and a continuum state (ground state $|0\rangle$). We assume that the dark mode does not couple with the external field, while geometrical parameters g_1 and g_3 indicate how strongly the bright mode and additional mode couple with the external field $E_0 = \tilde{E}_0 e^{i\omega t}$. We also define κ_{12} as the coupling parameter between $|1\rangle$ and $|2\rangle$, and κ_{23} as the coupling parameter between $|2\rangle$ and $|3\rangle$. The coupling between $|1\rangle$ and $|3\rangle$ is ignored due to their geometrical and functional similarity. Then, the field amplitude of all states can be described as a system of linearly coupled Lorentzian oscillators

a)Email: schen@nankai.edu.cn.
b)Email: jjtian@nankai.edu.cn.
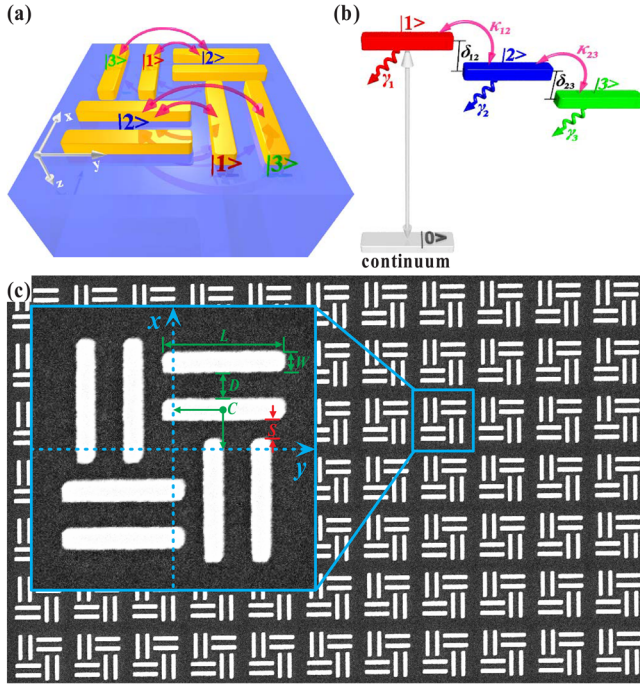
(a)

(b)

(c)

FIG. 1. (a) Unit cell of the PIT planar MM. The pink arrows indicate the near-field coupling between meta-atoms. (b) Coupled four-level plasmonic system for the PIT planar MM. (c) SEM of the sample with $S = 140$ nm. Inset: Amplified figure of the unit cell, showing the definitions of the geometrical parameters: $L = 900$ nm, $W = 150$ nm, $D = 200$ nm.

$$
\begin{bmatrix}
\omega - \omega_{01} + i\gamma_1 & \kappa_{12} & 0 \\
\kappa_{12} & \omega - \omega_{02} + i\gamma_2 & \kappa_{23} \\
0 & \kappa_{23} & \omega - \omega_{03} + i\gamma_3
\end{bmatrix}
\begin{bmatrix}
\tilde{A}_1 \\
\tilde{A}_2 \\
\tilde{A}_3
\end{bmatrix}
$$
$$
= -
\begin{bmatrix}
g_1 \tilde{E}_0 \\
0 \\
g_3 \tilde{E}_0
\end{bmatrix}. \tag{1}
$$

In Eq. (1), the complex amplitude of the bright mode $\tilde{A}_1$ is directly proportional to the polarizability of the PIT system. Therefore, the normalized energy extinction $P(\omega)$, namely the sum of reflection and absorption, is obtained as

$$
P(\omega) = \frac{|\tilde{A}_1|}{|\tilde{E}_0|} = \left| \frac{\frac{-g_3 \kappa_{12}\kappa_{23}}{(\omega - \omega_{02} + i\gamma_2)(\omega - \omega_{03} + i\gamma_3) - \kappa_{23}^2} - g_1}{(\omega - \omega_{01} + i\gamma_1) - \frac{\kappa_{12}^2(\omega - \omega_{03} + i\gamma_3)}{(\omega - \omega_{02} + i\gamma_2)(\omega - \omega_{03} + i\gamma_3) - \kappa_{23}^2}} \right|. \tag{2}
$$

The optimized structure was achieved by using the finite-element-method (FEM)-based commercial software COMSOL Multiphysics.[16] The parameters were chosen to match closely those of technologically feasible physical systems. The three-dimensional simulations were performed with a plane-wave source incident in the z direction. The refractive index of quartz substrate is 1.5. The optical constants of bulk gold in the infrared spectral regime are described by the Drude model with the plasma frequency $\omega_p = 2\pi \times 2.175 \times 10^{15} \mathrm{s}^{-1}$ and the damping constant $\omega_c = 2\pi \times 6.5 \times 10^{12} \mathrm{s}^{-1}$.[17] Owing to the surface scattering and grain boundary effects in the thin gold film, the damping constant in our simulations is three times larger than in bulk gold.[2,9] Periodic boundary conditions

were used for the x-y plane, and waveguide port boundary conditions were used on the other boundaries.

A series of samples were fabricated by standard E-beam deposition and E-beam lithography. First, a layer of ITO material (100 nm) was deposited on a 0.5-mm-thick quartz substrate by a RF magnetic sputtering system. The top patterned layer was defined with electron beam lithography. Then Cr (5 nm) and Au (100 nm) were deposited by an electron beam evaporator, and the pattern transfer was completed by lift-off in acetone. Both samples had a total area of $300\,\mu m \times 300\,\mu m$. Figure 1(c) shows the scanning electron microscopy (SEM) image of the fabricated PIT planar MM. It has a period of 2.1 μm in both the x and y directions. The top gold layer consists of eight identical gold bars. L and W are the length and width of the each bar, respectively. D is the fixed distance between two bars in each "=" pair. C is the coordinate of the inner bar. The interspace between two close "=" pairs is defined as S, which is 300 nm, 220 nm, 140 nm, and 60 nm for four samples, corresponding to the coordinate of C (375, 450) nm, (335, 410) nm, (295, 370) nm, and (255, 330) nm, respectively.

To study the PIT tuning feature of the designed PIT planar MM, we give the simulated and experimental transmission spectra as a function of the interspace S in Fig. 2. The PIT feature is apparent in the transmission spectra. The simulated transmission spectra obtained by FEM and four-level plasmonic system are shown in Fig. 2(a). The FEM simulation considers an x-polarized TEM beam normally incident to the PIT planar MM. There is a broad transmission dip in the case of maximum interspace $S = 300$ nm. Then, a tiny transmission peak emerges within the broad transmission dip with decreasing S. Finally, the transmission peak reaches $T(\omega) = 51.2\%$ at 2.85 μm in the case of minimum interspace $S = 60$ nm. The evolution of the PIT feature in the transmission spectra shows that the coupling strength between bright and dark modes strongly depends on S. We also fit the simulated transmission spectra according to $T(\omega) = 1 - P(\omega)$ from analytical derivation. This analytical derivation agrees closely with the FEM analysis for the different interspaces in Fig. 2(a), which confirms the validity of our design.

The transmission spectra were obtained at room temperature with a Fourier-transform infrared spectrometer (Bruker VERTEX 70, tungsten lamp) combined with an infrared microscope ($36\times$ magnification objective, liquid N$_2$-cooled MCT 77 K detector). The transmission of the sample was recorded by averaging data from 64 measurements to improve the signal-to-noise ratio. Before measuring the PIT sample, the transmission was calibrated with a blank structure without gold bars. The corresponding experimental transmission spectra in Fig. 2(b) agree qualitatively with the simulation. To show the variety of the PIT tuning feature, every graph shows the transmission spectrum of maximum interspace $S = 300$ nm along with different interspaces. We can see that the experimental results for $S = 300$ nm, 220 nm, and 140 nm agree closely with the simulation, while the experimental result for minimum interspace $S = 60$ nm is appreciably different from that of the simulation. These discrepancies between experiment and simulation are likely due to the fabrication tolerances such as the inhomogeneity of the interspace S especially for the sample with $S = 60$ nm. Considering that the optical properties of metamaterials with
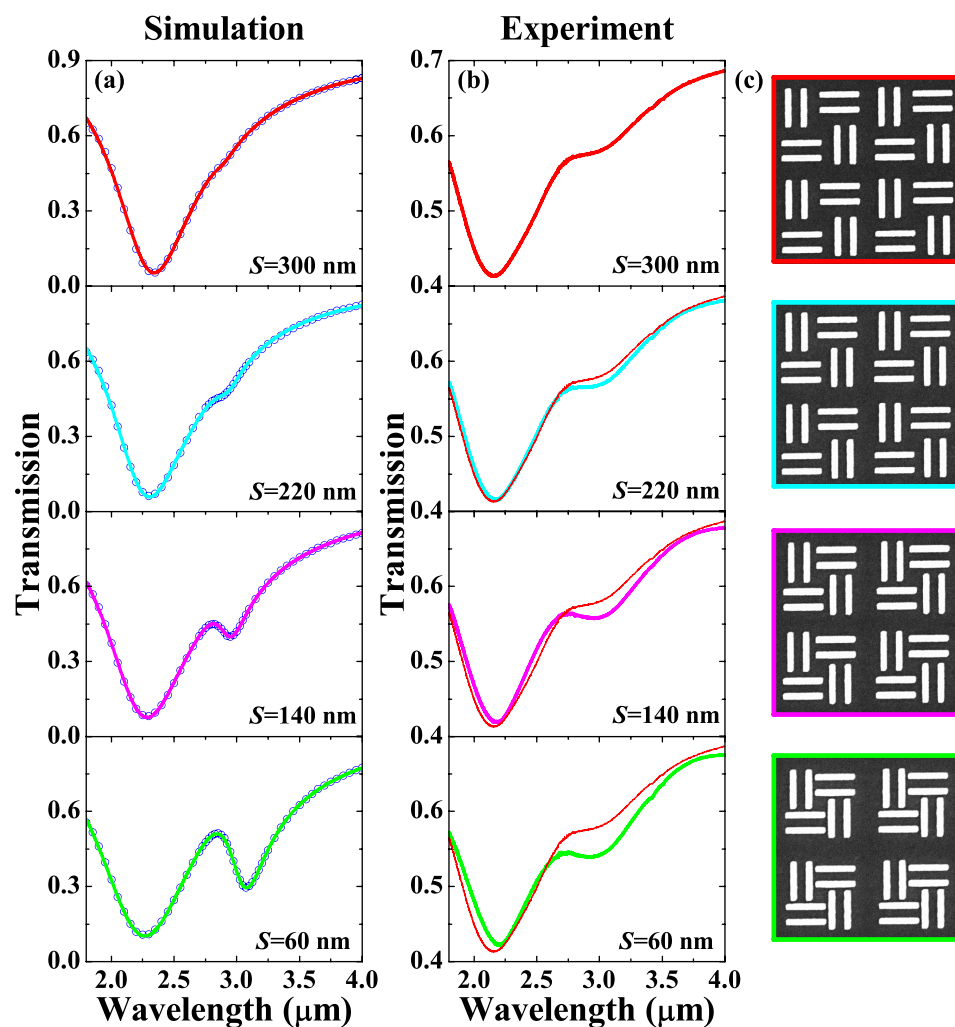
FIG. 2. (a) Simulated transmission spectra achieved by FEM (blue-circled curves) and four-level plasmonic system (color-solid lines) for different interspaces S. (b) Corresponding experimental transmission spectra. The transmission spectrum of $S = 300$ nm is shown in every graph by a fine red-solid line to guide the eyes. (c) Top-view SEM of the corresponding samples.

periodic structure are quite sensitive to the homogeneity, previous experimental attempts have not been successful owing to the difficulties with nanofabrication.[2,5] Even so, the experimental PIT tuning feature clearly agrees with the simulation for the $S = 300$ nm transmission spectrum in every graph. Therefore, our experimental results verify our analyses of the PIT phenomenon to a great extent.

To get insight into the nature of the designed PIT planar MM, we calculated the surface current density distribution and the magnetic field amplitude distribution of the top metallic layer for the x-polarized TEM wave with a 2.85-μm wavelength (see Fig. 3). The "=" pairs parallel to the y-axis, which may function as a magnetic quadrupole antenna,[18] can serve as the dark mode. The "=" pairs parallel to the x-axis, which may function as two similar optical dipole antennas,[19] can serve as the bright mode and additional mode. With the maximum interspace $S = 300$ nm (nearly without coupling to the dark mode), the bright mode and additional mode are strongly excited by the incident beam with a strong magnetic field and high surface current densities (as shown in Fig. 3(a)). By decreasing the interspace to 60 nm (with strong coupling to the dark mode), the magnetic field and surface
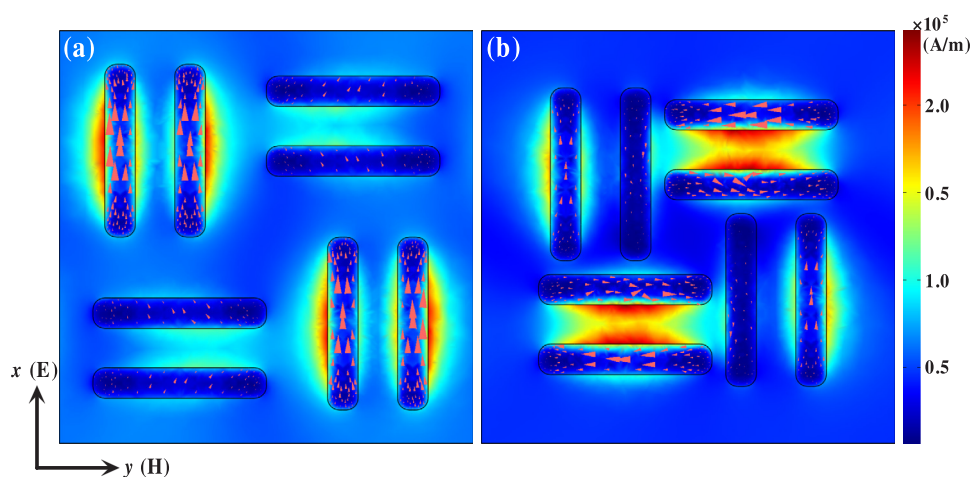

FIG. 3. Colormaps and pink arrows, respectively, represent the distributions of the amplitude of the magnetic fields and induced surface current densities of the top metallic elements at a 2.85-μm wavelength for (a) $S = 300$ nm and (b) $S = 60$ nm.
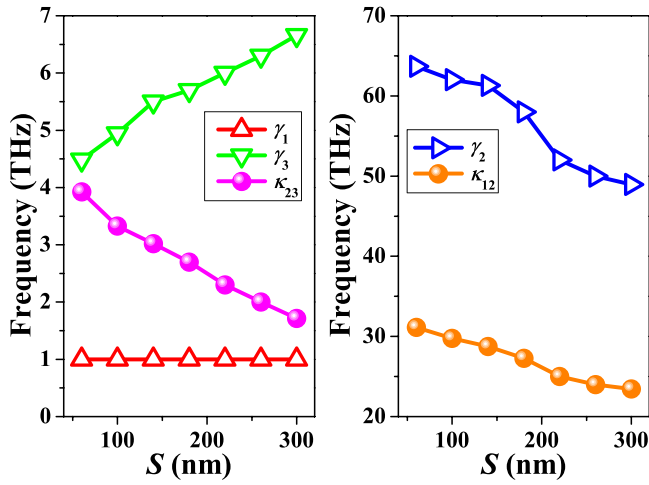
FIG. 4. Extracted simulated coupling and damping parameters as a function of interspace S. Values of γ_1, γ_2, γ_3, κ_{12}, and κ_{23} are extracted by fitting the simulated transmission spectra.

current are coupled back to the dark mode, leading to destructive interference and a suppressed state in the bright mode. Therefore, the magnetic field and surface current densities of the bright mode and additional mode decrease greatly (as shown in Fig. 3(b)), which corresponds to PIT. Because the additional mode is farther from the dark mode than the bright mode, the coupling strength between the additional mode and dark mode is weaker than that between the bright mode and dark mode. For all separations, the coupling among the bright, dark and additional modes leads to a narrow transmission peak in the broad dip.

To examine the coupling and damping parameters of our plasmonic system (see Fig. 1(b)), Fig. 4 shows the fitting values of γ_1, γ_2, γ_3, κ_{12}, and κ_{23} as a function of interspace S in frequency units. The resonant frequencies of the three modes are approximately $\omega_{01} = 125$ THz, $\omega_{02} = 119$ THz and $\omega_{03} = 100$ THz, respectively. We define $\delta_{12} = \omega_{01} - \omega_{02}$ and $\delta_{23} = \omega_{02} - \omega_{03}$ as the small detuning. Due to the positions of meta-atoms, the coupling between $|1\rangle$ and $|2\rangle$ is much stronger than between $|2\rangle$ and $|3\rangle$, which corresponds to $\kappa_{12} > \kappa_{23}$. Significantly, κ_{12} and κ_{23} are nearly inversely proportional to S, which determines the modulation strength of our PIT planar MM. The damping factors γ_1, γ_2, and γ_3 correspond to the decay rate in atomic physics, which is inversely proportional to spectral linewidth. As S decreases, the radiative damping component of γ_2 increases significantly, which means that the magnetic field and surface current are coupled back to the dark mode, leading to the emerging of the transmission peak. On the other hand, γ_1 and γ_3 are roughly constant, which agrees with the result that all linewidths of the spectrum are the same. Such quantitative results confirm our expectation about the relationship between the interspace and coupling strength of meta-atoms.

Polarization-insensitive performance and wide-angle incident beams are important in practical applications. In some cases, the most possible light needs to be used, which may contain arbitrarily polarized components. Moreover, the excited beam is not always normally incident to the sample in many cases. To show the polarization-insensitive behavior of the designed PIT planar MM, we plotted the transmission spectra as a function of polarization angle ϕ for $S = 300$ nm and $S = 60$ nm in Figs. 5(a) and 5(b), respectively. As the
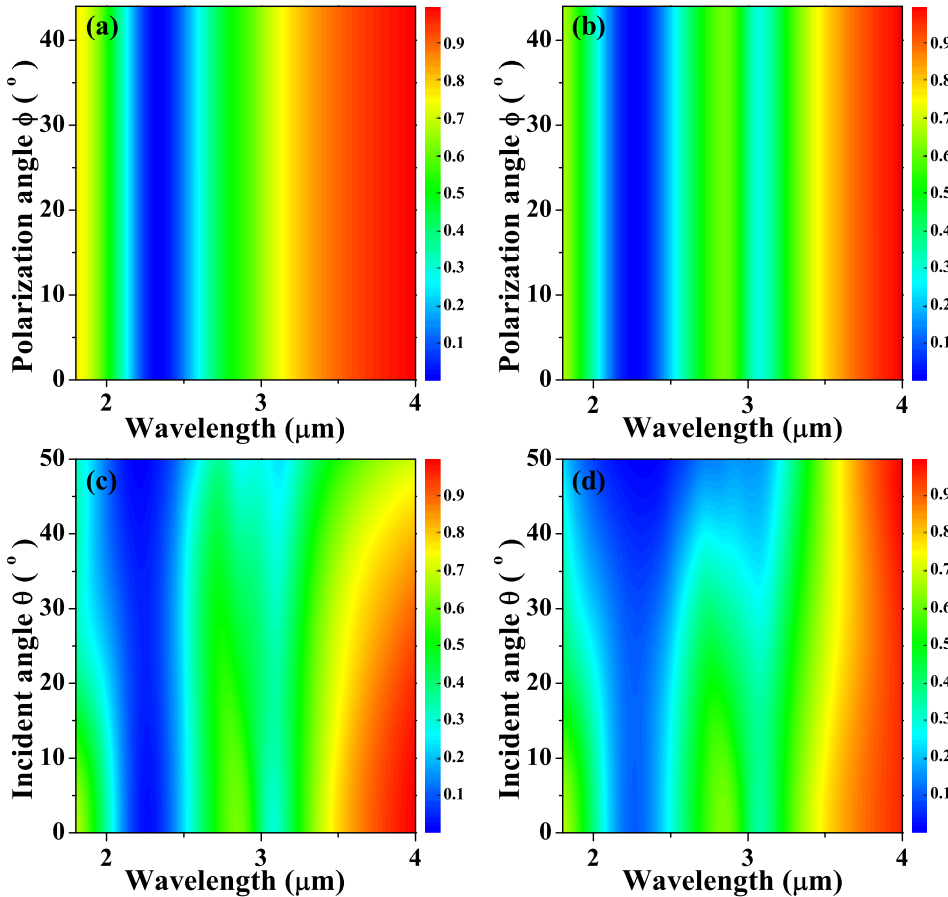

FIG. 5. Simulated transmission spectra as a function of wavelength and the polarization angle for (a) $S = 300$ nm and (b) $S = 60$ nm. Simulated angular dispersion of the transmission spectra for both (c) TE polarization and (d) TM polarization in the case of $S = 60$ nm.

PIT planar MM has a fourfold rotational symmetry, we only need to take into account the polarizations from $0°$ to $45°$ in the simulation. Results show that the transmission spectra of the designed PIT planar MM are polarization-insensitive. The PIT feature of the designed structure can also work over a wide range of incident angles θ. Figures 5(c) and 5(d) gives the simulated angular dispersion of the transmission spectra for TE and TM polarization for $S = 60$ nm, respectively. For the TE case, the PIT feature is nearly independent of incident angle, since the electric field can effectively provide the strong electric resonance at all incident angles. For the TM case, the PIT feature can be maintained with increasing the incident angle. However, when the incident angle is beyond $30°$, there is a monotonic decrease in the transmission. With increasing incident angle, the horizontal projection of the incident electric field decreases and can no longer efficiently drive a strong electric resonance. The maximal incident angle is about $10°$ in the previously designed PIT device;[20] however, our designed PIT planar MM maintains quite well for both TE and TM radiations over a wide range of incident angles.

In conclusion, we have numerically and experimentally demonstrated a PIT planar MM based on coupled meta-atoms. This shows that the local asymmetrical nanostructure leading to the plasmon-assisted interaction is the key to producing PIT, but it does not mean that PIT must depend on the polarization and the angle of incident waves. The analyses done have been kept general and so can be easily extended to other antenna geometries. This kind of PIT planar MM will help to overcome some of the limitations of customary designs developed so far. Our work offers a further step forward in developing optical modulation.

[1]S. Zhang, D. A. Genov, Y. Wang, M. Liu, and X. Zhang, Phys. Rev. Lett. **101**, 047401 (2008).

[2]N. Liu, L. Langguth, T. Weiss, J. Kästel, M. Fleischhauer, T. Pfau, and H. Giesson, Nature Mater. **8**, 758 (2009).

[3]A. Artar, A. A. Yanik, and H. Altug, Nano Lett. **11**, 1685 (2011).

[4]A. E. Çetin, A. Artar, M. Turkmen, A. A. Yanik, and H. Altug, Opt. Express **19**, 22607 (2011).

[5]R. Taubert, M. Hentschel, J. K'Stel, and H. Giessen, Nano Lett. **12**, 1367 (2012).

[6]M. Fleischhauer, A. Imamoglu, and J. P. Marangos, Rev. Mod. Phys. **77**, 633 (2005).

[7]B. Tang, L. Dai, and C. Jiang, Opt. Express **19**, 628 (2011).

[8]Z.-G. Dong, H. Liu, J.-X. Cao, T. Li, S.-M. Wang, S.-N. Zhu, and X. Zhang, Appl. Phys. Lett. **97**, 114101 (2010).

[9]N. Liu, T. Weiss, M. Mesch, L. Langguth, U. Eigenthaler, M. Hirscher, C. Sönnichsen, and H. Giessen, Nano Lett. **10**, 1103 (2010).

[10]J. Chen, P. Wang, C. Chen, Y. Lu, H. Ming, and Q. Zhan, Opt. Express **19**, 5970 (2011).

[11]P. Tassin, L. Zhang, T. Koschny, E. N. Economou, and C. M. Soukoulis, Phys. Rev. Lett. **102**, 053901 (2009).

[12]L. Zhang, P. Tassin, T. Koschny, C. Kurter, S. M. Anlage, and C. M. Soukoulis, Appl. Phys. Lett. **97**, 241904 (2010).

[13]Q. Xu, S. Sandhu, M. L. Povinelli, J. Shakya, S. Fan, and M. Lipson, Phys. Rev. Lett. **96**, 123901 (2006).

[14]J. B. Lassiter, H. Sobhani, M. W. Knight, W. S. Mielczarek, P. Nordlander, and N. J. Halas, Nano Lett. **12**, 1058 (2012).

[15]V. Yannopapas, E. Paspalakis, and N. V. Vitanov, Phys. Rev. B **80**, 035104 (2009).

[16]COMSOL *Multiphysics User's Guide*, Version 3.5 (Comsol AB, Brulington, MA, 2008).

[17]M. A. Ordal, L. L. Long, R. J. Bell, S. E. Bell, R. R. Bell, R. W. Alexander, Jr., and C. A. Ward, Appl. Opt. **22**, 1099 (1983).

[18]V. M. Shalaev, W. Cai, U. K. Chettiar, H.-K. Yuan, A. K. Sarychev, V. P. Drachev, and A. V. Kildishev, Opt. Lett. **30**, 3356 (2005).

[19]L. Novotny, Phys. Rev. Lett. **98**, 266802 (2007).

[20]Y. Lu, X. Jin, S. Lee, J. Y. Rhee, W. H. Jang, and Y. P. Lee, Adv. Nat. Sci.: Nanosci. Nanotechnol. **1**, 045004 (2010).